Scientia Iranica B (2022) 29(2), 478–485

Sharif University of Technology
Scientia Iranica
Transactions B: Mechanical Engineering
http://scientiairanica.sharif.edu

Analysis of loading distribution for SRB and TSRB combined bearing

L. Shi[a,b,*], J. Wang[a,b], K. Luo[a,b], D. Feng[a,b,*], H. Zhang[a,b], and E. Miao[c]

a. *School of Mechanical Engineering, Yangtze University, Hubei Jingzhou, 434023, China.*
b. *Hubei Engineering Research Center of Oil and Gas Drilling and Completion Tools, Jingzhou 434023, China.*
c. *College of Mechanical Engineering, Chongqing University of Technology, Chongqing 401135, China.*

Received 14 July 2020; received in revised form 24 February 2021; accepted 25 October 2021

KEYWORDS
Combined bearing;
Bearing washer;
Loading distribution;
Numerical simulation;
Finite element analysis.

Abstract. Combined bearings are made of spherical roller and thrust spherical roller bearings that are two important supports in different low-speed heavy-duty mechanisms, and the stability of their running state is the key to ensure supporting the normal operation of the mechanism. Based on the functionality of wellbore trajectory control tool, the loading distribution of the combined bearing under pure radial and axial forces is theoretically studied. Two kinds of the limit state of the rolling elements movement called "Odd press" state and "Even press" state are considered, and the Hertzian line elastic contact model is used to deal with the contact between roller and raceway. The calculation results of the contact stress and radial displacement are very close to the analysis results, and the accuracy of the analysis results is verified by the radial displacement experiment. The results indicate that the radial load causes the radial displacement of the combined bearing axis, which is about 5.81×10^{-3} mm. The radial displacement can affect the guiding accuracy of the tool to a certain extent. The radial displacement can be reduced by adjusting the structural dimensions of the combined bearing. The findings of this research can be employed to design combined Spherical Roller Bearing (SRB) and Thrust Spherical Roller Bearing (TSRB) combined bearings in actual engineering problems.

1. Introduction

Combined bearing is specially designed and manufactured for different industrial applications. It can bear both radial and axial loading. Due to the difference of loading direction, lubrication condition, and dustproof requirements, many series combinations are available for designers to select [1]. In order to change the direction of the bit while keeping its rotation unaffected, the wellbore trajectory control tool needs the combined bearing to support the rotation and deflection of tool spindle.

In the 1970s, combined bearings were formed to meet the demands of high-performance drilling applications. Zhuo [2] developed a high-speed spherical bearing with good results. Halliburton [3] incorporated a spherical roller bearing into the combination of two thrust spherical roller bearing forms proposed by Japan National Oil Corporation to mitigate the bit impacts on the bearing and enable it to withstand higher temperature and speed requirements.

The combined bearing of the wellbore trajectory control tool consists of a Spherical Roller Bearing (SRB) and two Thrust Spherical Roller Bearings (TSRB), as shown in Figure 1. The raceway of the

*. *Corresponding authors. Tel.: +86 15927864976 (L. Shi); +86 13607219921 (D. Feng)*
E-mail addresses: shilei0909@163.com (L. Shi); fengd0861@163.com (D. Feng)

doi: 10.24200/sci.2021.56408.4710

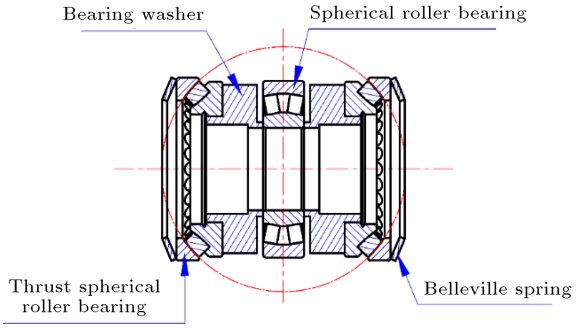

Figure 1. Combined bearing structure diagram.

two TSRB outer ring forms the first sphere of the tool spindle for rotation and deflection. The raceway of SRB outer ring forms the second sphere to correct this rotation and deflection. Under the condition of borehole trajectory control tool deflection, the combined bearing deflects with the tool spindle. The outer ring raceways of the thrust self-aligning roller bearing at both ends form an outer sphere to support the deflection of the spindle, and those of the central self-aligning roller bearing form an inner sphere to support the deflection of the spindle. The deflection of the tool spindle occurs under the joint support of the inner and outer spheres formed by the combined bearing. In the drilling processes, the working state of the bearing change with the bending of the spindle. In case the bearing stress exceeds its endurance, the bearing will fail [4,5]. The study of the loading distribution for SRB and TSRB combined bearing in wellbore trajectory control tool is very significant to ensure the proper drilling and design of combined bearing.

2. The theoretic study of loading distribution for SRB and TSRB combined bearing

2.1. The force distribution under pure radial loading

Prior to the study of radial loading distribution of bearings, first, two kinds of limit state of bearing movement should be taken into account. In the state shown in Figure 2(a), the radial loading action line goes through the center of rolling elements. The number of rolling elements which contact with raceway at this time can only be an odd number; this state is called the "odd press" state. In the state shown in Figure 2(b), the loading just acts on the bisector of the angle between two rolling elements. The number of rolling elements which contact with raceway at this time can only be an even number; this state is called the "even press" state [6].

Based on the classical bearing analysis theory, the theory of rigid ring is adopted [7,8]. This assumption greatly simplifies the analysis process, and its calculation results enjoy certain precision. Therefore, the

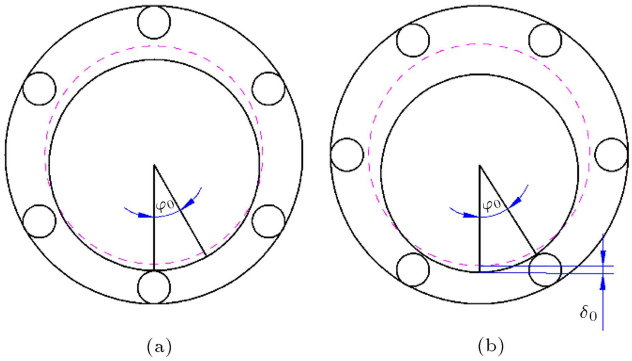

Figure 2. Two types of limit state of rolling elements movement: (a) "Odd press" state and (b) "Even press" state.

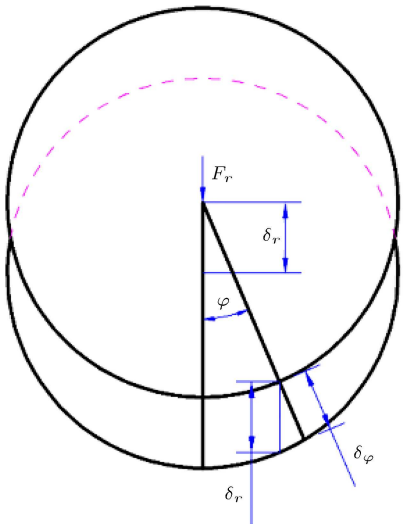

Figure 3. The radial displacement of component.

combination bearing in the wellbore trajectory control tool was analyzed based on which the above assumption was adopted.

As shown in Figure 3 the inner and outer circles of the bearing considered the produced relative displacement δ_r under the action of radial force F_r. In this respect, the displacement component at any position angle φ is as follows:

$$\delta_\varphi = \delta_r \cos\varphi. \tag{1}$$

Prior to loading to the bearing, certain measures are usually taken to preload the bearing; this can reduce the bearing clearance to zero or make it negative. In this way, the bearing stable operation can be ensured. Therefore, when building mathematical models, we can assume that the bearing radial clearance is zero. In Figure 4, the normal component of radial displacement $\delta_{r\varphi}$ is:

$$\delta_{e\varphi} = \delta_{r\varphi} \cos\alpha_e = \delta_r \cos\varphi \cos\alpha_e. \tag{2}$$

According to the relation between loading and displacement, $Q_{e\varphi}$ force is calculated through the following

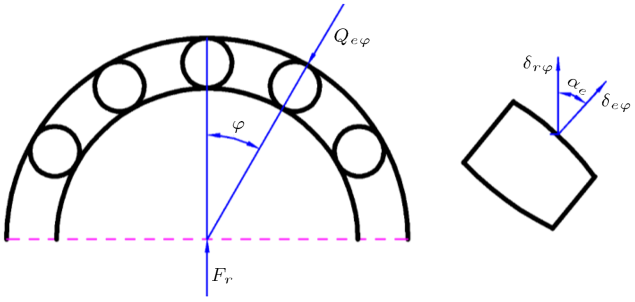

Figure 4. Displacement distribution under typical contact.

equation:

$$Q_{e\varphi} = K\delta_{e\varphi}^{\varepsilon}, \tag{3}$$

where K is the stiffness coefficient whose value is derived from the following formula [9]:

$$K = 2.89 \times 10^4 l^{0.82} D_w^{0.11},$$

where l (mm)is the length of the rolling element; D_w (mm) is the equivalent diameter of the rolling element. The exponent ε can be selected based on the bearing type. Since the two types of bearings in this study are roller bearing, the value of ε is 10/9. In Eqs. (2) and (3), the relation between the normal force of rolling elements $Q_{e\varphi}$ at the position angle φ and the biggest normal force of the rolling element Q_e is as follows:

$$Q_{e\varphi} = Q_e(\cos\varphi)^{10/9}. \tag{4}$$

Under the condition of the contact, the equilibrium equation can be established as follows:

$$F_r - \sum_{\varphi\geq-\pi/2}^{\varphi\leq\pi/2} Q_{e\varphi}\cos\alpha_e\cos\varphi = 0. \tag{5}$$

The above equation only considers the loading situation when φ ranges from $-\frac{\pi}{2}$ to $\frac{\pi}{2}$ as $\delta_{r\varphi} \leq 0$ when φ is in another scope.

If we assume that the number of the rolling elements is Z, the equilibrium equation under "odd press" state is as follows:

$$F_r = \sum_{\varphi\geq-\pi/2}^{\varphi\leq\pi/2} Q_{e\varphi}\cos\alpha_e\cos\varphi = Q_e Z J_{ra}\cos\alpha_e. \tag{6}$$

Therefore, the following equation can be obtained:

$$Q_e = \frac{F_r}{ZJ_{ra}\cos\alpha_e}, \tag{7}$$

where J_{ra} is the radial loading distribution coefficient under "odd press" state, which is calculated as follows:

$$J_{ra} = \frac{1}{Z}\left\{1 + 2\sum_{\varphi=2\pi/Z}^{\varphi\leq\pi/2}(\cos\varphi)^{19/9}\right\}. \tag{8}$$

The equilibrium equation under the "even press" state is as follows:

$$F_r = \sum_{\varphi\geq-\pi/2}^{\varphi\leq\pi/2} Q_{e\varphi}\cos\varphi = Q_e Z J_{rb}\cos\alpha_e. \tag{9}$$

Therefore, we have:

$$Q_e = \frac{F_r}{ZJ_{rb}\cos\alpha_e}. \tag{10}$$

In the "even press" state, Q_e does not exist, and the actual maximum loading appears in a pair of rolling elements which is the closest distance to the load line. It can be measured as:

$$Q'_e = Q_e\left[\cos\left(\frac{\pi}{z}\right)\right]^{10/9}. \tag{11}$$

2.2. The force distribution under pure axial loading

Under the action of pure axial loading, the inner and outer circles of bearing produce a relative displacement δ_a, as shown in Figure 5. Here, the contact loading and displacement of the rolling elements are the same. When the outer ring is fixed, the rolling elements and outer ring generate contact displacement under the action of axial displacement. The contact force of the rolling elements is referred to as Q_e. The normal contact displacement is δ_e and the contact angle is α_e.

The normal contact displacement caused by the axial force is:

$$\delta_e = \delta_a\sin\alpha_e. \tag{12}$$

Therefore, the contact loading of the rolling element can be obtained in the following:

$$Q_e = K\delta_e^{10/9} = K\delta_a^{10/9}(\sin\alpha_e)^{10/9}. \tag{13}$$

Consequently, the axial direction of the components of the contact loading is determined below:

$$\begin{aligned} Q_{ea} &= Q_e\sin\alpha_e = K\delta_a^{10/9}(\sin\alpha_e)^{10/9}\sin\alpha_e \\ &= K\delta_a^{10/9}(\sin\alpha_e)^{19/9}. \end{aligned} \tag{14}$$

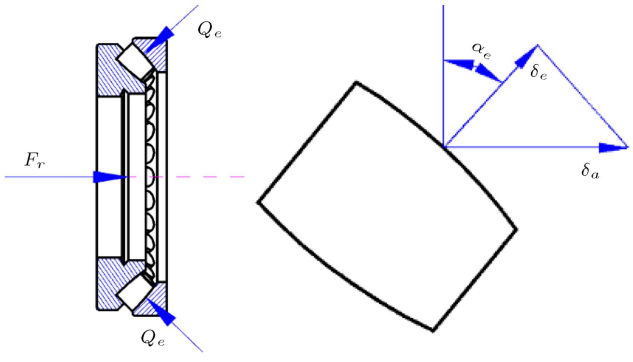

Figure 5. Distribution of loading.

Table 1. Wellbore trajectory control tool with combined bearing structural parameters.

Name of parameters	Parameter value	Unit
SRB bearing contact angle, α_e	10.2	°
SRB bearing outer diameter, D_{mo}	155	mm
SRB bearing inner diameter, D_{mi}	70	mm
Number of rollers for SRB bearing, Z_m	18	/
TSRB bearing contact angle, α_t	45	°
TSRB bearing outer diameter, D_{to}	155	mm
TSRB bearing inner diameter, D_{ti}	70	mm
Number of rollers for TSRB bearing, Z_t	21	/
length of rolling element, l	11.67	mm
Equivalent diameter of rolling element, D_w	16.30	mm

Suppose that the number of the rolling elements of the bearing is Z; then, the equilibrium equation is obtained as follows:

$$F_a - ZK\delta_a^{10/9}(\sin\alpha_e)^{19/9} = 0. \tag{15}$$

The axial displacement can be obtained in the following:

$$\delta_a = \left(\frac{F_a}{ZK(\sin\alpha_e)^{19/9}}\right)^{9/10}. \tag{16}$$

2.3. Structural parameters, loads and calculation results

2.3.1. Combined bearing structural parameters and loads

As shown in Table 1, combined bearing structural parameters are employed to calculate the stiffness coefficient. Under the condition of steering drilling, the radial force that transfers to combined bearing is 12733 N and the axial force is 1089 N, which is derived from the earlier research on wellbore trajectory control tool [10].

2.3.2. Calculation results

Using Eqs. (1)–(16), we can calculate the contact load for each bearing, as shown in Tables 2 and 3.

Based on the classical Hertz elastic contact theory, the maximum contact stress between the roller and raceway is about 312.1 MPa, and the radial displacement is about 2.7×10^{-3} mm.

Table 2. Load distribution of SRB.

φ (°)	0	±20	±40	±60	±80
Q_φ (N)	2938.00	2741.80	2184.97	1360.11	419.99

3. The Finite Element Analysis (FEA) of SRB and TSRB combined bearing

There are two kinds of working states when wellbore trajectory control tool is exposed to typical working condition, i.e., the normal drilling and steering drilling. In normal drilling, the spindle only sustains the axial bit pressure and it does not bend. On the contrary, in steering drilling, the spindle sustains the axial bit pressure as well as the radial force applied by eccentric mechanism. This radial force leads to spindle bending. Therefore, during the FEA of both SRB and TSRB combined bearings, two cases appear.

3.1. Modeling, material selection and meshing of combined bearing

Due to the complexity of the combined bearing structure and wide contact area, it would be not only time-consuming, but also difficult to modify the application of the finite element software. In order to improve the efficiency of modeling, the Solidworks software is employed to establish a three-dimensional model of bearing [11,12]. In this regard, this study used the multi-physics field analysis software COMSOL for analyzing the load situation of the combined bearing under two kinds of working conditions, namely typical drilling and steering drilling.

The relatively high-speed rotation and vibration are generated in the operation of wellbore trajectory control tool. On the one hand, the rolling elements must withstand the repeatedly alternating stress; on the other hand, there is a relative slip between the rolling elements and race. In this situation, the rolling elements with good mechanical properties are required.

Table 3. Load distribution of TSRB.

φ (°)	0	±12.86	±25.71	±38.57	±51.43	±64.29	±77.14
Q_φ (N)	2627.02	2553.93	2339.59	1998.48	1554.16	1038.83	494.67

For this reason, bearing steel was selected as the bearing material in this research [13,14].

For the contact area, the manner of local refinement was employed to ensure the accuracy of calculation.

3.2. Adding boundary conditions

Given that the radial, tangential, and axial freedoms of bearing race that contact with the shell are limited, the three bearing races need to be added to the fixed constraint. In addition, the spindle only sustains the axial bit pressure under normal working conditions. Here, the combined bearing only sustains the pre-tightening force. Therefore, under typical working conditions, the race of two thrust spherical roller bearings should be added with an axial force of 1089 N.

Under the condition of steering drilling, the spindle not only sustains the bit pressure but generates bending. Based on the mechanical analysis of the spindle [15,16], it can be concluded that the eccentric ring needs to be added with the radial force of 16918 N when the spindle generates maximum deflection. However, the radial force transferred to the combined bearing is 12733 N. Therefore, when conducting boundary loading, the shaft circle of spherical roller bearing as well as the inside of two gaskets should be added with the radial force of 12733 N. At the same time, both ends of the thrust spherical roller bearing should also be added with the pre-stressing force of 1089 N.

All the data above including axial force (1089 N) and radial force (12733 N) were taken from the earlier research on the wellbore trajectory control tool, which was supported by the National Natural Science Foundation of China (51275057).

3.3. Results and analysis

3.3.1. The results and analysis of normal drilling

To obtain bearing under loading simulation, the main focus was placed on the rolling element behavior. Based on the above pre-treatment and solution procedure, the stress and displacement diagram of the combined bearing during typical drilling can be obtained, as shown in Figures 6 and 7.

The effect of pre-stressing force is observable on the stress and displacement distributions. The maximum stress on the thrust spherical roller bearing is placed, reaching the value of 2.94 MPa. In addition, the displacement of the thrust spherical roller bearing inside race is also obvious. The dimensions of the largest displacement are 5.85×10^{-5} mm.

According to the pictures, the loading is formed by all rolling elements evenly under the effect of axial pre-tightening force. This finding is consistent with the theoretical study results in Section 2.2 under pure axial loading when the stress is mainly concentrated in the contact area between the rolling element and raceway;

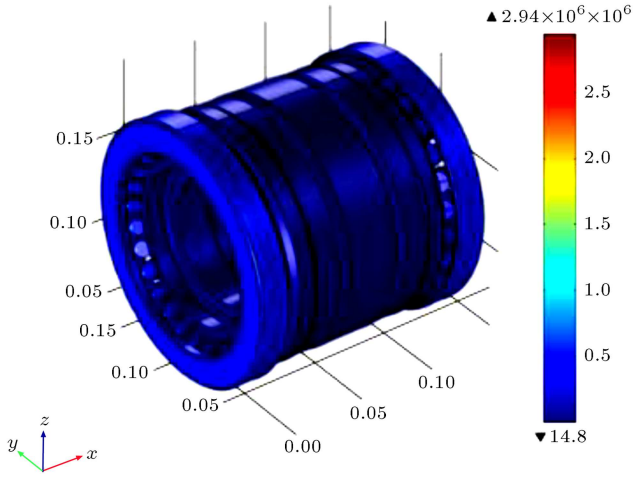

Figure 6. Von Mises stress distribution (Pa).

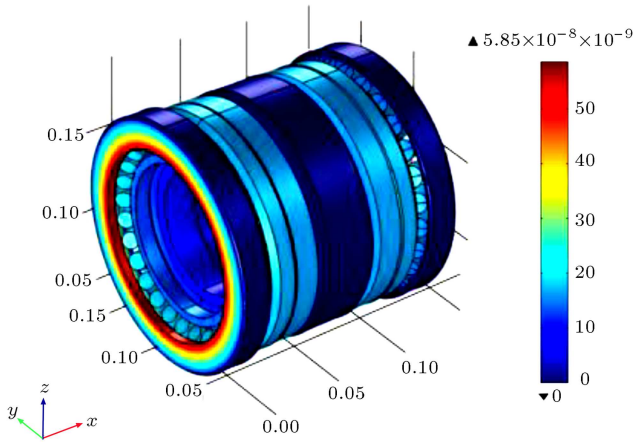

Figure 7. Displacement distribution (m).

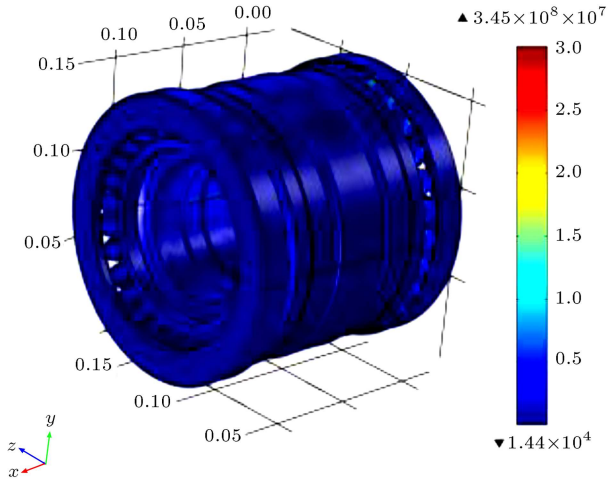

Figure 8. Steering drilling stress (Pa).

3.3.2. The results and analysis of steering drilling

Under steering drilling conditions, the stress and displacement distributions in the combined bearing are shown in Figures 8–11.

In the stress and displacement distribution of

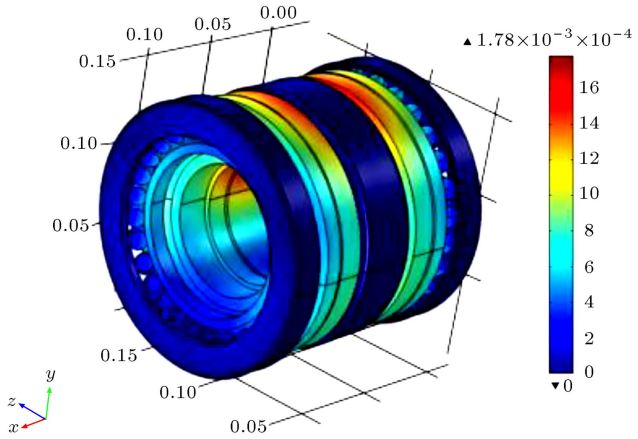

Figure 9. Steering drilling displacement (m).

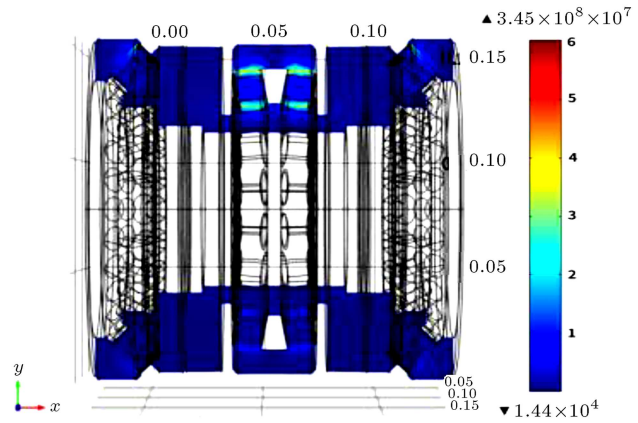

Figure 10. Stress of XY plane (Pa).

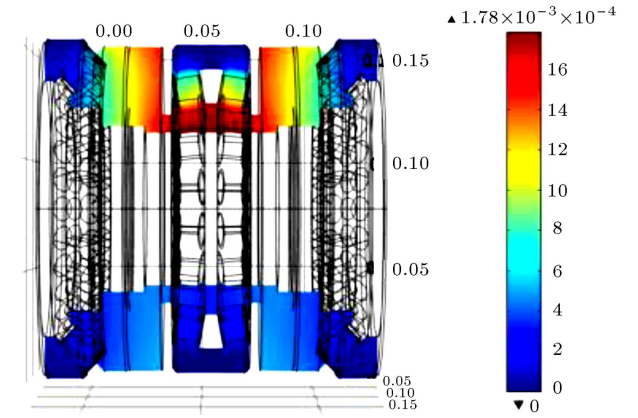

Figure 11. Displacement of XY plane (m).

the combined bearing, a large amount of stress and displacement in the radial load line of the rolling element and raceway contact parts takes place when the outer ring is fixed. The stress value away from the area gradually decreases. In this case, the maximum stress value is 345 MPa and the biggest displacement is 1.78×10^{-3} mm.

According to the analysis results, the loading response of bearing is mainly focused on the contact area of both rolling element and raceway. Further, under the action of radial force, the upper circle rolling element is larger, while the under circle rolling element remains almost unaffected by the loading. In addition, the rolling element loading distribution is "being large in the middle and small at both ends". In steering drilling, the values of the radial force and axial force are 12733 N and 1089 N, respectively. Here, the effect of the axial force on the rolling element loading response is quite insignificant and the action of pure radial load is considered to be the condition of steering drilling. Under pure radial loading, this finding is consistent with the theoretical study results in Section 2.1.

Table 4. Summary of the combined bearing results.

The result type	Contact stress	Radial displacement
Calculation results	312.1 MPa	2.7×10^{-3} mm
Simulation results	345 MPa	1.78×10^{-3} mm
Experimental results	—	5.81–5.95×10^{-3} mm

Figures 10 and 11 show the stress and displacement distributions of the section that crosses the axis as well as the radial loading action line of the combined bearing. Accordingly, the loading that spherical roller bearing sustains is larger than the thrust spherical roller bearing. The stress mainly concentrates on the contact between the rolling element and raceway. In addition, under the action of radial loading, the gasket generates an axial compression to the thrust spherical roller bearing on both sides. This compression in turn makes the thrust spherical roller produce secondary stress. Therefore, in order to reduce the stress concentration of bearing, the bearing washer should be conducted with a reasonable design.

3.3.3. The comparative results of the experimental, computational, and finite element methods

It is difficult to measure the contact stress between the roller and raceway based on the experiments conducted under actual working conditions. A research study [5] elaborates the experiment method and presents the experimental results of the wellbore trajectory control tool. Table 4 summarizes the results of calculation, simulation, and experiments.

A comparison between the experimental and calculated results, and simulation results reveal that radial displacement results obtained from the three methods are very close to each other. Tool weight and uncontrollable factors such as machining error make the experimental results more significant than the analysis results.

4. Conclusion

In this paper, the formula for the bearing's loading

distribution was derived from the combined SRB and TSRB bearing of wellbore trajectory control tool. The three-dimensional model of combined bearing was established using Solidworks software. The loading situation of the combined bearing was analyzed by the COMSOL software. After making a comparison between theoretical study results and FEA results, the following conclusions can be obtained:

1. When the combined bearing sustained pure axial force, the loading response was evenly taken by the rolling element. Moreover, much of the pre-tightening force was sustained by thrust spherical roller bearing, while the spherical roller bearing was almost not affected by loading. Therefore, the mechanical properties of thrust spherical roller bearing should be superior to those of the spherical roller bearing;
2. When the SRB and TSRB combined bearing sustained pure radial force, the loading response of rolling element was the most significant through the action line, which is at the center of the bearing. The loading on both sides of bearing was reduced and the stress remained mainly concentrated in the contact part between the rolling elements and raceway. Therefore, the mechanical behavior of rolling elements and raceway should be seriously taken into consideration in the structure design of combined bearing;
3. The secondary stress on both sides of the bearing is generated by the radial load of the bearing washer. In order to reduce the stress concentration of bearing, the structure of the bearing washer needs to be reasonably designed to prolong the service life of bearing in the next step.

Acknowledgement

This research was supported by the scientific research program of Hubei Education Department (Q20181315) and Hubei Technology Innovation Project (major project) (2019AAA010) as well as Yangtze University Excellent Master Degree Thesis Cultivation Program (YS2018023).

Nomenclature

SRB	Spherical Roller Bearing
TSRB	Thrust Spherical Roller Bearings
δ_r	Radial displacement
$\delta_{r\varphi}$	Normal component of radial displacement
K	Stiffness coefficient
$Q_{e\varphi}$	Normal force of rolling elements
l	Length of rolling element
J_{ra}	Radial load distribution coefficients for "odd press"
δ_e	Normal contact displacement
F_r	Radial force
φ	Any position angle
α_e	Contact angle
$\delta_{e\varphi}$	Normal displacement of rolling elements
D_w	Equivalent diameter of rolling element
Q_e	The rolling elements' contact force
Z	The number of the rolling elements
ε	Coefficient by bearing type
δ_a	Axial displacement

References

1. Huang, L.L., Xue, Q.L., Liu, B.L., et al. "Dynamic reliability analysis of rotary steering drilling system", *Mechanical Sciences*, **10**(1), pp. 79–90 (2019).
2. Peng, S.S. "Contact stress analysis for self-aligning bearings of guide drilling system", **Bearing**, **14**, pp. 7-9 (2014).
3. Ikeda, A. and Shano K. "Device for controlling the drilling direction of drill", bit: U.S. Patent 5,875,859[P], 1999-3-2.
4. Feng, D., Lu, C., Zhang, H., et al. "Research on control of steering movement of well trajectory control tool", *Journal of Oil Field Equipment*, **46**, pp. 6–10 (2017).
5. Zhang, H., Feng, D., Wei, S.Z., et al. "A new predicting method of build-up rate of steering tools based on kriging surrogate model", *Arabian Journal for Science and Engineering*, **43**(9), pp. 4949–4956 (2018).
6. Huang, H.J., Wang, X., and Xue, K.J. "Effect of cage wear in rolling bearing on bearing failure", *Journal of Lubrication Engineering*, **46**(07), pp. 128–136 (2021).
7. Wang, Y., Tse, P.W., Tang, B.P., et al. "Order spectrogram visualization for rolling bearing fault detection under speed variation conditions", *Mechanical Systems and Signal Processing*, **122**, pp. 580–596 (2018).
8. Vashisht R.K. and Peng, Q.J. "Crack detection in the rotor ball bearing system using switching control strategy and short time Fourier transform", *Journal of Sound and Vibration*, **432**, pp. 502–529 (2018).
9. Harris, O.O. and Osisanya, S.O., *Evaluation of Equivalent Circulating Density if Drilling Fluids Under High-Pressure/High-Temperature Conditions*, SPE, 97018 (2015).
10. Shi, L., Wang, K.Q., Feng, D., et al. "Wellbore trajectory control tool seal system leakage analysis based on steady gap flow", *Advances in Mechanical Engineering*, **12**, p. 6 (2020).
11. Dong, Y.X., Si, D.H., and Liu, W.S. "Research on parametric design of high-speed spindle", *Journal of*

Mining & Processing Equipment, **47**(02), pp. 47–52 (2019).

12. Ma, S.J., Yan, K., Zhang, X.H., et al. "An accurate modeling method and secondary development of bearing contact-motion", *Journal of Xi'an Jiaotong University*, **55**(08), pp. 33–41 (2021).
13. Bombač, D., Terčelj, M., Peruš, et al. "The progress of degradation on the bearing surfaces of nitrided dies for aluminium hot extrusion with two different relative lengths of bearing surface", *Wear*, **307**, pp. 1–2 (2014).
14. Muzakkir, S.M., Lijesh, K.P., and Hirani, H. "Tribological failure analysis of a heavily-loaded slow speed hybrid journal bearing", *Engineering Failure Analysis*, **40**, pp. 12–24 (2014).
15. Feng, D., Lv, J.H., Xiang, Z.X., et al. "Failure analysis an optimization of cantilever bearing of borehole trajectory control devices", *Journal of Science Technology and Engineering*, **16**, pp. 179–182 (2016).
16. Zhang, H., Xiang, Z.X., Qian, L.Q., et al. "The correlation between the spindle load and the deflecting capacity of the wellbore trajectory control tool", *Journal of Mechanics in Engineering*, **39**, pp. 152–157 (2017).

Biographies

Lei Shi received his PhD in Engineering from Changjiang University in 2017. Specializing in oil field equipment, he has published several papers and participated in the translation of a series of books on foreign oil and gas exploration and development progress. He has participated in six projects at national and provincial levels and published eight first-author academic papers in relevant academic journals.

Jiangang Wang is currently a PhD Student at Yangtze University. He received his Ms degree at Yangtze University in 2021. As a major participant, he has participated in three national provincial and ministerial projects and published four related papers. His research interests include theoretical and technical applications in the design, diagnosis, and dynamic simulation of petroleum machinery.

Kai Luo was admitted to the School of Mechanical Engineering, Yangtze University for Ms degree in September 2019. Among the participants involved in the two national natural science foundations of China, he is mainly responsible for structure simulation and test-related jobs. His research interests include mechanical system simulation and diagnosis technology.

Ding Feng is a Professor of Mechanical Engineering at Yangtze University, China. He received his PhD at the China University of Petroleum (Beijing). His main research areas are design, testing, and diagnostics of oil and gas drilling, completion tools, equipment and offshore engineering equipment, tubular column mechanics, and dynamic simulation technology. He has participated in nearly 90 projects at national and provincial levels and published 179 relevant academic papers.

Hong Zhang is an Associate Professor, Supervisor to Master's students, and the Director of Hubei Mechanical and Electrical Engineering Society. She has participated in more than six vertical projects of provincial and ministerial level sources such as subprojects of major special projects of MIIT, Hubei Provincial Department of Education, State Key Laboratory and Hubei Provincial Key Laboratory, etc. She has also published more than 20 papers and more than 20 patents. Her research interests are petroleum equipment research and development.

Enming Miao is a Professor and a PhD Supervisor at the School of Instrument Science and Optoelectronic Engineering at the Hefei University of Technology. His main research interests are precision mechanical engineering, accuracy theory, thermal error compensation of CNC machine tools, and structural design theory and application technology of mechanical thermal robustness. He has published more than 50 papers.